ISSN 0965-545X, Polymer Science, Ser. A, 2011, Vol. 53, No. 7, pp. 546–557. © Pleiades Publishing, Ltd., 2011.
Original Russian Text © E.S. Trofimchuk, A.V. Efimov, N.I. Nikonorova, A.L. Volynskii, N.F. Bakeev, L.N. Nikitin, A.R. Khokhlov, L.A. Ozerina, 2011, published in Vysokomolekulyarnye Soedineniya, Ser. A, 2011, Vol. 53, No. 7, pp. 1020–1032.

Crazing of Isotactic Polypropylene in the Medium of Supercritical Carbon Dioxide[1]

E. S. Trofimchuk[a], A. V. Efimov[a], N. I. Nikonorova[a], A. L. Volynskii[a], N. F. Bakeev[a], L. N. Nikitin[b], A. R. Khokhlov[b], and L. A. Ozerina[c]

[a] *Faculty of Chemistry, Moscow State University, Moscow, 119991 Russia*
[b] *Nesmeyanov Institute of Organoelement Compounds, Russian Academy of Sciences, ul. Vavilova 28, Moscow, 119991 Russia*
[c] *Karpov Institute of Physical Chemistry, ul. Vorontsovo pole 10, Moscow, 105064 Russia*
e-mail: elena_trofimchuk@mail.ru

Received September 30, 2010;
Revised Manuscript Received January 11, 2011

Abstract—Uniaxial tensile drawing of films based on semicrystalline isotactic PP in the medium of supercritical carbon dioxide at a pressure of 10 MPa and a temperature of 35°C is studied. The tensile drawing of PP is shown to proceed in the homogeneous mode without necking and is accompanied by intense cavitation. The maximum level of porosity is 60 vol %. The porous structure that develops owing to the tensile drawing of the polymer in supercritical CO_2 is provided by formation of a set of crazes that are primarily localized in interlamellar regions. According to small-angle X-ray scattering data, the average diameter of fibrils that bridge craze walls changes slightly with an increase in tensile strain and is ~10 nm; the specific surface of the craze fibrils is 100–150 m^2/cm^3.

DOI: 10.1134/S0965545X11050154

INTRODUCTION

Crazing is one of the modes of plastic deformation of amorphous and semicrystalline polymers [1–3]. Nucleation and the subsequent growth of crazes are markedly enhanced in the presence of liquid media that reduce the surface energy of polymers [2]. Under the above conditions, crazing is the key mechanism of inelastic deformation of solid amorphous and semicrystalline polymers.

Glassy polymers usually experinece classical solvent crazing [4]. In this case, crazes with a thickness varying from fractions of a micron to tens of microns nucleate. The crazes are separated by long fragments of the initial undeformed material and can cross the entire cross section of the sample. The craze walls are bridged by oriented fibrils with a diameter of 10–20 nm that are separated by voids of nearly the same dimensions [3, 4].

In addition, semicrystalline polymers undergo another mode of crazing referred to as delocalized (or intercrystallite) crazing. This mode of crazing is accompanied by the development of interconnected fine crazes with a thickness of several tens of nanometers, and these crazes are primarily localized in the interlamellar regions of the semicrystalline polymer [2, 5–7]. This mode of solvent crazing is traditionally observed for the tensile drawing of highly crystalline polymers in liquid media at temperatures above the glass-transition temperature of the amorphous phase. In this case, the mechanical characteristics of the amorphous and crystalline phases are substantially different, for example, in HDPE [6] and isotactic PP [7]. Note that all structural and morphological aspects of delocalized solvent crazing are far from being well studied.

Tensile drawing of polymers via the mechanism of crazing can proceed also in gaseous media. For example, according to [8], classical crazes form during tensile drawing of isotactic PP in the presence of various gases (N_2, O_2, CO_2) at atmospheric pressure (0.1 MPa) in the broad temperature interval from –196 to –60°C. Gases were shown to be effective crazing-promoting agents only at temperatures 10–20°C higher than their condensation or sublimation (in the case of CO_2) temperatures. A further temperature rise markedly decreases the potency of gases as crazing-promoting agents. In this case, the deformation behavior of the polymers becomes similar to that in vacuum. In [8], two possible mechanisms of action of a gas on a deformed polymer have been advanced: (i) a decrease in the surface energy of the formed fibrils that is due to gas adsorption and (ii) enhanced plastic deformation of the polymer provided by the plasticiz-

[1] This work was supported by the Russian Foundation for Basic Research (project nos. 10-03-00827 and 10-03-90030); by the Division of Chemistry and Materials Science, Russian Academy of Sciences, under the basic-research program Development of New Metallic, Ceramic, Glassy, Polymeric, and Composite Materials; by the Presidium of the Russian Academy of Sciences (Program P21); by the State Program for Support of Leading Scientific Schools (NSh-4371.2010.3); and under State Contract no. 02.740.11.0143.

ing action of the gas in the craze tip. As the temperature increases, the adsorptional activity of a gas decreases and its solubility in the polymer becomes lower; as a result, its crazing-promoting ability goes down.

In fact, according to [9], there is a critical relative gas pressure $p/p_s = 0.20–0.25$ (p_s is the pressure corresponding to gas condensation at a given temperature) below which no classical crazes form. At this pressure, a monolayer of sorbed gas on a flat surface arises. The maximum craze-growth rate is attained at $p/p_s \sim 0.60–0.80$, at which several polylayers form on the polymer surface. It was assumed in [10] that the adsorptive action of the gas requires its condensation in the formed cavities, that is, formation of a liquid phase.

In recent years, the interest of researchers has been focused on problems of the interaction between polymers and gaseous media above the critical temperature and under the action of high pressure (above 5 MPa). The distinctive features of supercritical fluids are the absence of gas/liquid interfaces and the prohibition of the liquid phase. Under certain conditions, these fluids combine the characteristics of a liquid (its ability to dissolve solids, high density) and a gas (low viscosity, low surface tension).

Of special interest is the study of interaction between polymers and supercritical carbon dioxide [11], which has low critical parameters ($T_{cr} = 31.8°C$, $p_{cr} = 7.4$ MPa). At temperatures above the critical temperature and at a pressure of 10–30 MPa, it shows good thermodynamic affinity toward all linear commercial polymers.

There are several publications [12–15] devoted to the tensile drawing of various polymer films and fibers in a supercritical fluid. They can be conditionally divided into two basic groups: (i) postorientational drawing for the preparation of high-modulus fibers based on PET, PA-6, and ultrahigh-molecular-weight PE [12, 13] and (ii) preparation of highly porous polymer films and fibers with submicronic and micronic pores [14, 15].

In this study, supercritical carbon dioxide is used as a crazing-promoting medium. In this case, this approach offers an evident advantage for the replacement of traditional liquid media, which usually are organic solvents (alcohols, hydrocarbons, amines, etc.), with ecologically friendly, fireproof, and explosion-proof fluids. Of special attraction are the simple procedure of removing CO_2 from the volume of polymers after their stretching and the absence of any capillary phenomena that usually lead to marked structural rearrangements of the unstable crazed structure. Moreover, in comparison to the densities of conventional gaseous media, the density of supercritical carbon dioxide can be varied in a broad range, thereby achieving the density of liquids [11]. These specific features of supercritical carbon dioxide allow fine adjustment of the activity of the medium.

Earlier [16, 17], we studied the specific features of uniaxial tensile drawing of commercial films of various polymers in the medium of supercritical carbon dioxide (a pressure of 10 MPa, a temperature of 35°C). This approach allowed development of a porous structure in certain polymer films (PP and HDPE). We assumed that, in this case, the formation and development of an open porous structure proceeds via the mechanism of crazing. However, the mechanism of this process remains unclear.

The objectives of this study are the comprehensive investigation of the mechanism of crazing and the detailed characterization of the structure formed during uniaxial stretching of films based on isotactic PP in the medium of supercritical carbon dioxide. For this purpose, various structural and mechanical approaches were used. For example, the method of small-angle X-ray scattering was used to calculate the parameters of the porous structure. The solution of the posed problems presents evident interest not only for description of the mechanism of deformation of polymers in specific fluids that are supercritical gases but also for prediction of physicomechanical characteristics of materials used under given conditions.

EXPERIMENTAL

Two types of commercial films based on isotactic PP were studied.

First, isotropic PP-1 film ($M_w = 3 \times 10^5$, the film thickness was 120–140 μm) prepared via melt extrusion was studied. The initial film was annealed in the free state at 140°C for 3 h. After annealing, the polymer sample had a melting temperature of 165°C and a degree of crystallinity of 65%.

Second, a slightly oriented extrusion film based on PP-2 ($M_w = 1.5 \times 10^5$, the film thickness was 60–80 μm) was studied. The initial film was annealed in its free state at 150°C for 1 h. After annealing, the polymer had a melting temperature of 165°C and a degree of crystallinity of 65%.

The annealed PP samples had a monoclinic structure of crystallites. Optical-microscopic observations did not reveal any spherulites in the test films.

The uniaxial tensile drawing of the PP samples in the medium of CO_2 was performed in a specially designed stretching labscale device.[2] Standard dumbbell-shaped specimens with a gage size of 6 mm × 20 mm were used. A schematic presentation and a photograph of the experimental setup are shown in Fig. 1. A pressure generator (High Pressure Equipment, United States) with a volume of 90 ml was used to achieve a pressure gradient of up to 30 MPa. A set of

[2] This experimental setup was designed and constructed jointly by Moscow State University (Laboratory of Structure of Polymers, Division of High-Molecular-Mass Compounds, Faculty of Chemistry) and the Nesmeyanov Institute of Organoelement Compounds, Russian Academy of Sciences.

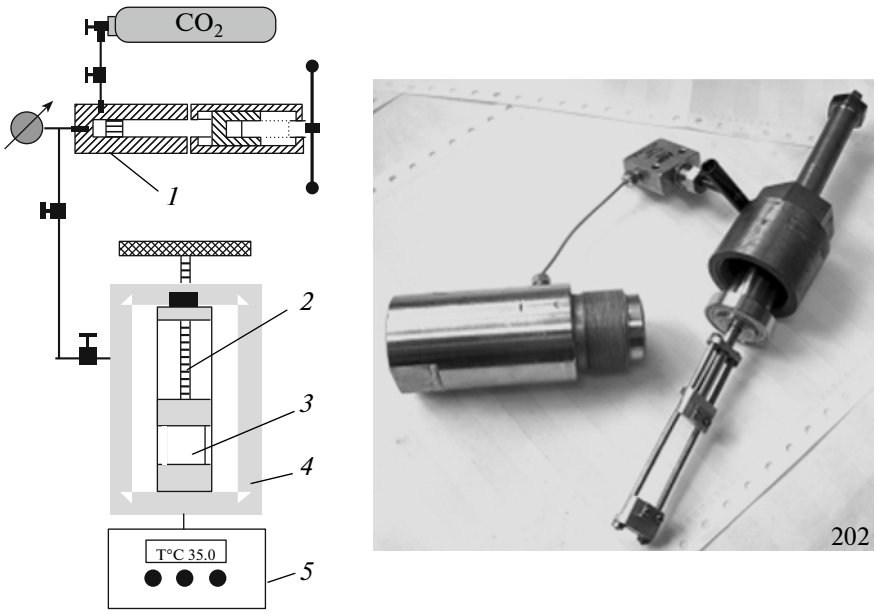

Fig. 1. Scheme of the experimental setup and a photograph of the high-pressure chamber for the uniaxial tensile drawing of polymers in supercritical media: (*1*) syringe pressure generator, (*2*) stretching device, (*3*) sample, (*4*) high-pressure cell, (*5*) temperature sensor and heater.

valves provided the supply of CO_2 to the cell. The pressure generator and the cell were equipped with mechanical manometers that made it possible to monitor pressure in the system as well as gas inflow and outflow.

Prior to each experiment, the high-pressure cell with the sample fixed in clamps was thermostated at 35°C for 30 min; then, the cell was filled with CO_2 (reagent grade), the pressure was adjusted to the desired level, and the sample was thermostated for another 10 min. The working pressure was varied from 0.1 to 10 MPa. Then, the sample was stretched by a given tensile strain (from 10 to 400%). The strain rate was 25%/min. Then, CO_2 was removed from the volume of the polymer samples by reducing pressure below the critical point by releasing gas through the valve.

The volume porosity was estimated from changes in the geometrical dimensions of PP samples after tensile drawing in the CO_2 medium. The measurements were conducted at normal pressure when the samples were released from the cell in which they were stretched (the samples were fixed in clamps in the stressed state). Volume gain $\Delta V/V_0$ was calculated through the equation $\Delta V/V_0 = (V_f - V_0)/V_0$, where V_0 is the initial volume of the polymer sample and V_f is its final volume.

The reversible character of deformation of the PP samples in the CO_2 medium was studied according to the following procedure. The polymer sample was stretched in CO_2 at a pressure of 10 MPa by a given tensile strain, and the sample was unloaded. Then, the sample was removed from the cell, released from the clamps, and allowed to relax in the free state at normal pressure for 2 days. The relative shrinkage in the longitudinal direction, a, was estimated as the ratio between the reversible strain and preliminary strain of the sample according to the equation $a = (l_1 - l_2)/(l_1 - l_0) \times 100\%$, where l_0 is the initial length of the sample, l_1 is the length of the stretched sample, and l_2 is the length of the sample after shrinkage.

The mechanical tests were performed at room temperature and at atmospheric pressure on an Instron-4301 universal tensile machine. The crosshead speed was 25%/min.

The morphology of the stretched samples was studied by scanning electron microscopy. To this end, to prevent shrinkage in the longitudinal direction, the films stretched in the medium of supercritical carbon dioxide were fixed by length in the stretching clamps. Then, the fixed sample was cooled in liquid nitrogen and subjected to brittle fracture so that the fractured sample stayed in the fixed state in the stretching clamps. Then, the fractured surface was decorated with gold and examined on a Hitachi S-520 scanning electron microscope.

The small-angle X-ray patterns of the initial and CO_2-stretched PP samples were collected on a Nanostar (Bruker AXS) instrument with a two-dimensional coordinate detector (CuK_α radiation, point collimation of the primary beam). The angular resolution was 8′.

In addition, X-ray studies were conducted on a KRM-1 diffractometer with slit beam collimation (Ni-filtered CuK_α radiation). The angular resolution was 6′. The scattering intensity in absolute units was

estimated with the use of the Kratky reference standard.

The curves of SAXS intensity distribution in the meridional direction were constructed via the scanning of X-ray patterns collected in an X-ray chamber with slit collimation. As the scattering coordinate, the modulus of the scattering vector was used: $s = 2\sin(\varphi/2)\lambda$, where φ is the scattering angle and $\lambda = 0.154$ nm is the wavelength of X-ray radiation. The constructed distribution curves were normalized by the primary beam intensity, the exposure, and the thickness of the sample.

The thermophysical characteristics of the samples (melting temperature, heat of fusion, degree of crystallinity) were estimated by the DSC method. The measurements were performed with a DSC-30 cell on a Mettler TA4000 thermal analyzer in the temperature interval 25–250°C; the heating rate was 10 K/min. The collected thermograms were analyzed with the original software of a Mettler-TC11 instrument.

RESULTS AND DISCUSSION

Tensile Drawing of the PP Films in the Medium of Supercritical CO_2

Let us consider the evolution of deformation of isotropic PP-1 films in the medium of supercritical CO_2. Deformation of the PP films under the above conditions proceeds homogeneously without necking and is accompanied by intense whitening of the sample. In this case, the samples show a relatively small narrowing of the gage size. Note that tensile drawing of PP-1 films in air or in the medium of gaseous CO_2 at a pressure of 0.1 MPa is accompanied by necking.

Figure 2 (point *1*) shows volume gain $\Delta V/V_0$ of the PP-1 samples plotted against the tensile strain after tensile drawing of the polymer sample in supercritical CO_2. Tensile drawing of the film under the above conditions is accompanied by intense cavitation. The sample volume increases at a tensile strain of about 10%. The value of $\Delta V/V_0$ nearly linearly increases as tensile strain increases up to 60–80%. At higher tensile strains, porosity increases at a slower rate and reaches a maximum value of 60 vol %.

The deformation of anisotropic PP-2 samples in the medium of supercritical CO_2 proceeds similarly. (The samples were stretched along the direction of extrusion.) The curves describing changes in the volume porosity as a function of tensile strain practically coincide for PP-1 and PP-2 (Fig. 2, points *1*, *2*). Note that the tensile drawing of the anisotropic PP-2 film in air proceeds homogeneously without any necking but is not accompanied by intense development of porosity. For example, the volume porosity of the PP-2 samples after stretching in air by 100% does not exceed 2–4 vol %. It seems that, in this case, plastic deformation without any violation of the integrity of the material dominates.

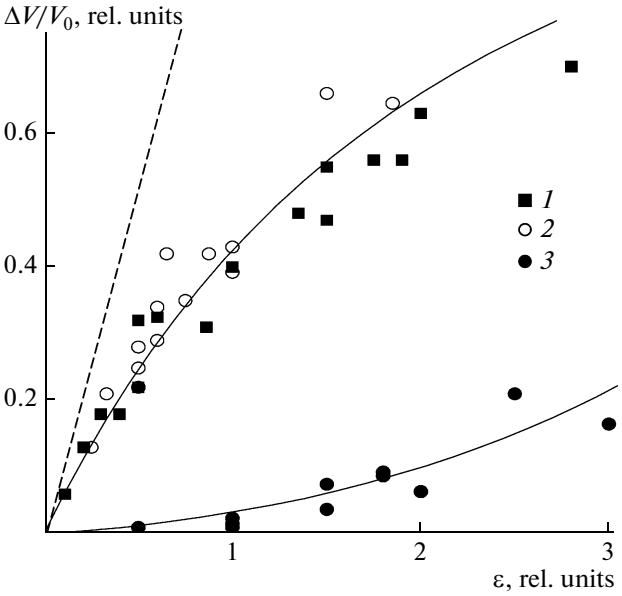

Fig. 2. Volume gain of the sample plotted against relative tensile strain (*1*, *2*) for the PP-1 and PP-2 samples after tensile drawing in the medium of supercritical CO_2 and (*3*) for the PP-1 sample after tensile drawing in supercritical CO_2 and the subsequent shrinkage. The dashed line is the theoretical dependence calculated under the assumption that deformation proceeds solely via the mechanism of crazing.

It was shown earlier that, after tensile drawing in the medium of supercritical CO_2, PP films are permeable to low-molecular-mass liquids. In this case, the effective pore diameter estimated according to Poiseuille's equation is 4–10 nm for the polymer samples after tensile drawing by 50–300% [16]. As follows from the literature data, the development of nanoscale pores is a feature of the deformation of semicrystalline polymers accompanied by craze formation [2, 7, 18]. According to the SAXS data, the lateral dimensions of the pores between fibrils in the crazes formed during the tensile drawing of semicrystalline polymers (HDPE, PP) in liquid environments are 5–25 nm [19, 25]. Therefore, it may be expected that tensile drawing of PP samples in contact with supercritical CO_2 proceeds via the mechanism of solvent crazing.

The morphology of PP films stretched in the CO_2 medium was studied via scanning electron microscopy. The structure of the samples was found to be sufficiently homogeneous. The SEM image of the fractured surface does not show the classical crazed structure with well-pronounced crazes separated by regions of the bulk polymer. Note also that the SEM image does not reveal any cellular pores, which are usually produced owing to the exposure of polymers, including PP, in supercritical CO_2 [21, 22]. It seems that, in this case, the so-called delocalized mode of solvent crazing occurs. This mode of solvent crazing primarily comes into play for the tensile drawing of semicrystal-

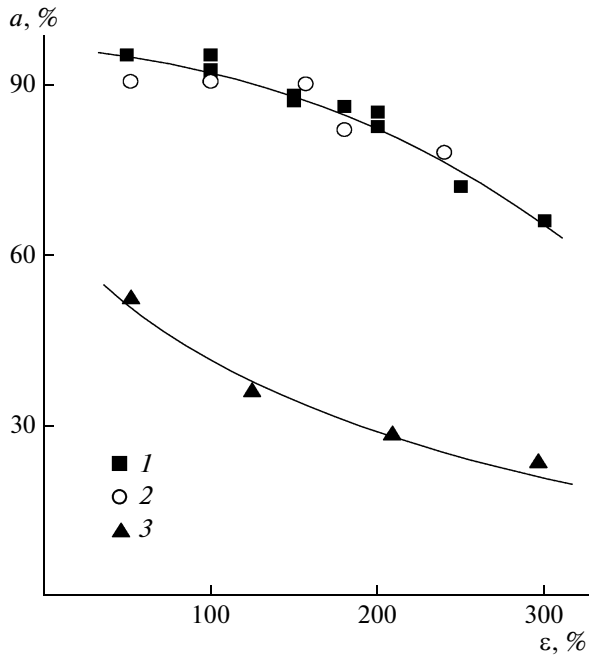

Fig. 3. Shrinkage plotted against relative tensile strain for (*1*) PP-1 and (*2*, *3*) PP-2 samples after tensile drawing (*1*, *2*) in supercritical CO_2 and (*3*) in air.

line polymers (including PP and HDPE) in active liquid media that are able to induce partial swelling [4–7].

Mechanical Behavior of Porous PP Films

Conclusions about the development of crazes are confirmed also by the study of the mechanical behavior of PP samples after tensile drawing in the supercritical medium. It is known that structural instability is a feature of crazed materials. After tensile drawing via the mechanism of solvent crazing, the samples based on glassy amorphous and semicrystalline polymers have the ability to recover their dimensions during unloading, a phenomenon that is provided by the "closure" of crazes [2].

For example, the shrinkage of HDPE and PP samples after stretching in liquid AALE by several hundred percent achieves 80–95% with respect to the preliminary tensile strain of the polymer sample [23]. Marked shrinkage is likewise typical for air-stretched semicrystalline polymers (HDPE, isotactic PP, polyoxymethylene) that are structured as hard elastic materials; in this case, shrinkage is 90–95% [24].

In this study, the shrinkage of PP films after tensile drawing in the supercritical medium was investigated. Figure 3 (points *1*, *2*) plots the relative shrinkage for the PP-1 and PP-2 samples after tensile drawing in the CO_2 medium against the relative tensile strain of the polymer sample. For comparison, Fig. 3 illustrates the dependence of the shrinkage of the anisotropic PP-2 sample in air (points *3*). Note also that the shrinkage of the fully necked isotropic PP-1 sample (at a tensile strain of 250–300%) is low and comes to 20–25%.

Figure 3 shows that the tensile drawing of the PP samples in the supercritical medium is highly reversible. After the tensile drawing of the films in supercritical carbon dioxide by 50–150%, the shrinkage of the films during fast unloading is 87–95% with respect to the initial tensile strain. As the tensile strain of the PP samples in CO_2 increases to 300%, the shrinkage markedly decreases to 65%. However, in the interval of tensile strains, the shrinkage of the samples after tensile drawing in CO_2 is much higher than the shrinkage of the air-stretched samples.

We measured the porosity of the PP-1 samples preserved after the tensile drawing of the polymer sample in CO_2 and the subsequent shrinkage (Fig. 2, points *3*). As follows from Fig. 2, the recovery of the initial dimensions is accompanied by a decrease in the volume of microvoids formed during the tensile drawing of the polymer sample. This observation makes it possible to conclude that the shrinkage of the film is due to the presence of crazes formed owing to the tensile drawing of the polymer sample in CO_2.

Coming back to the data on changes that occur in the volume fraction of pores as the relative tensile strain of the PP sample in supercritical CO_2 changes (Fig. 2), note the following result. When deformation fully proceeds via the mechanism of crazing (cavitation), the sample experiences no lateral deformation and the dependence of the volume fraction of pores on the relative tensile strain should be described by the dashed straight line shown in Fig. 2. Then, the volume porosity should increase in proportion to the relative tensile strain of the polymer sample. The marked deviation of the experimental data from the theoretical dependence indicates that the tensile drawing of PP in CO_2 proceeds both via the mechanism of solvent crazing and via shearing, which does not lead to any increase in the volume of the sample.

The high level of relative shrinkage (85–95%) after the tensile drawing of the PP sample in CO_2 by tensile strains of 50–200% (Fig. 3, points *1*, *2*) suggests that, in this interval of tensile strains, the crazing mechanism dominates.

A decrease in the relative shrinkage of the polymer samples after tensile drawing by tensile strains exceeding 150–200% is related to a higher contribution from deformation via the mechanism of shearing without any pore formation. However, the fraction of crazing remains high, as evidenced by a sufficiently high level of shrinkage of the PP samples after tensile drawing in CO_2 (Fig. 3).

The development of crazes during the tensile drawing of isotactic PP in supercritical CO_2 imparts unique mechanical characteristics that are not typical of crystalline polymers. Figure 4 presents the stress–strain curves for the isotropic PP-1 samples recorded during

tensile drawing in air after preliminary stretching in CO_2 and subsequent shrinkage. The subsequent tensile drawing of these sample proceeds homogeneously; this process is not accompanied by necking, and the resultant samples become milky white. The profiles of the repeated stress–strain curves for the PP-1 film stretched in CO_2 by more than 50% are different from the profile of the stress–strain curve of the initial polymer: The repeated curve is lower than the initial curve and is S-shaped. In this case, the $\sigma-\varepsilon$ curve shows two steps: the first step at low tensile strains and the second step at tensile strains nearly corresponding to the initial tensile strain of the polymer in CO_2. Within this interval of ε, the repeated curve coincides with the stress–strain curve of the initial PP.

The shrinkage of the PP samples after stretching in CO_2 and repeated tensile drawing in air is much greater than the shrinkage of the initial samples of the semicrystalline polymer. This conclusion follows from the data presented in Fig. 5, which shows the repeated stress–strain curves in the cyclic loading regime for the PP-1 samples after tensile drawing in CO_2 by 100% and shrinkage in the free state. For comparison, Fig. 5 presents the stress–strain curves in the cyclic loading regime for the initial PP-1 film. Indeed, during the reverse movement of crossheads, the relative shrinkage of the deformed sample stretched by $\varepsilon = 50\%$ is 80% with respect to the initial tensile strain; at $\varepsilon = 100\%$, this shrinkage is ~75%. The levels of shrinkage of the initial PP-1 samples stretched by the same tensile strains are much lower: 50 and 35%, respectively.

This evidence suggests that the repeated tensile drawing of the crazed PP-1 in air likely proceeds via opening of crazes that form during the tensile drawing of the sample in CO_2 and collapse during free-standing drying. In this case, the highly dispersed fibrillar structure of crazes is partially regained. Earlier, similar stress–strain curves of the repeated tensile drawing were recorded for several amorphous and semicrystalline polymers after tensile drawing via solvent crazing [2]. This evidence indicates a common mechanism of deformation of the polymer in supercritical CO_2 and adsorptionally active liquid media.

Therefore, this study of the mechanical response of the films after stretching in the medium of supercritical CO_2 verifies the assumption that the development of the porous structure in PP, as in the case of that in AALE, proceeds via the mechanism of solvent crazing.

Structure of Porous PP Films Deformed in the Medium of Supercritical CO_2

For a more detailed study of the porous structure induced in PP films after tensile drawing in supercritical CO_2, the small-angle X-ray scattering procedure was used. Figures 6a and 7a show the SAXS curves for the initial samples of isotropic PP-1 and anisotropic PP-2 samples. The initial isotropic PP-1 film is characterized by an angular X-ray reflection with a nearly

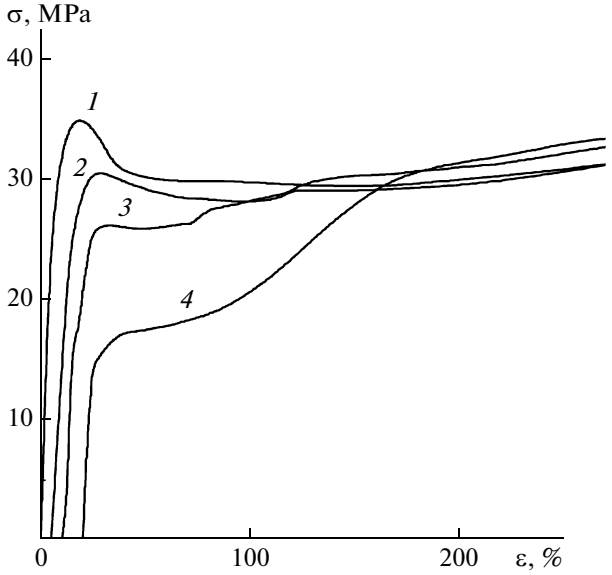

Fig. 4. The stress–strain curves recorded in air at room temperature (*1*) for the initial PP-1 sample and (*2–4*) for the polymer samples after tensile drawing in supercritical CO_2 by tensile strains of (*2*) 50, (*3*) 100, and (*4*) 180% and shrinkage in the free state. The curves are shifted along the abscissa axis toward the residual strain.

homogeneous intensity distribution along the circle. The long period calculated according to the Wolf–Bragg equation $L = \lambda/\varphi_{max}$ (where λ is the wavelength of X-ray radiation and φ_{max} is the angle corresponding to the maximum of the curve) was 24 nm.

The anisotropic PP-2 film is characterized by an arc X-ray reflection (the long period is 22–24 nm) that is contracted to the meridian of the X-ray pattern (Fig. 7a). This evidence indicates that, in the extruded films, the lamellas are primarily oriented perpendicularly to the direction of tensile drawing. The existence of a certain orientation of crystallites in the extruded PP-2 films is confirmed by the fact that the 040 and 130 reflections in the corresponding WAXS pattern appear as arcs contracted to the equator.

The development of crazes leads to a marked increase in the small-angle X-ray scattering intensity relative to that of the initial undeformed polymer. The SAXS patterns for both isotropic and anisotropic PP samples after tensile drawing in CO_2 show two types of scattering: a more intense scattering in the shape of a dumbbell (fan) that is localized in the meridional regions and a less intense equatorial scattering that is elongated in the direction perpendicular to the direction of tensile drawing (Figs. 6b, 7b). Earlier, similar SAXS patterns were recorded for solvent-crazed PP films [18, 20].

The boundaries of the meridional scattering along the direction of tensile drawing approach the angular position of the X-ray reflection from the undeformed polymer. The meridional scattering is assumed to arise

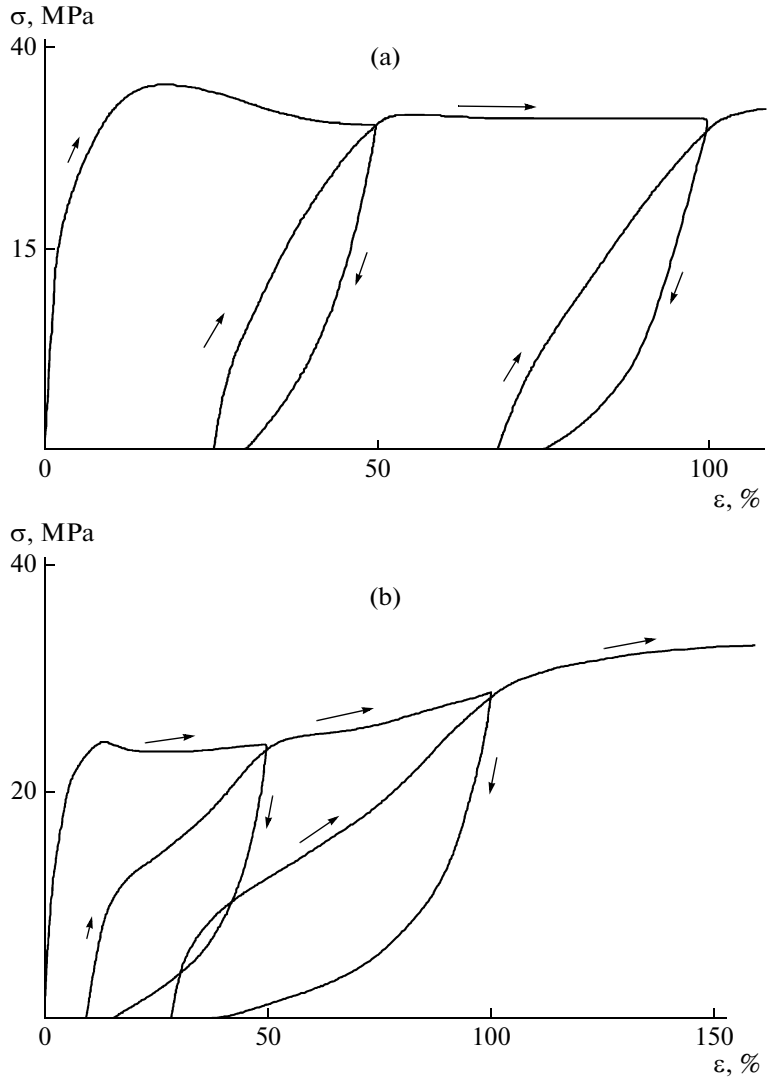

Fig. 5. Stress–strain curves recorded in the cyclic loading mode in air at room temperature (a) for the initial PP-1 sample and (b) for the sample after preliminary tensile drawing in the medium of supercritical CO_2 by 100% and subsequent shrinkage.

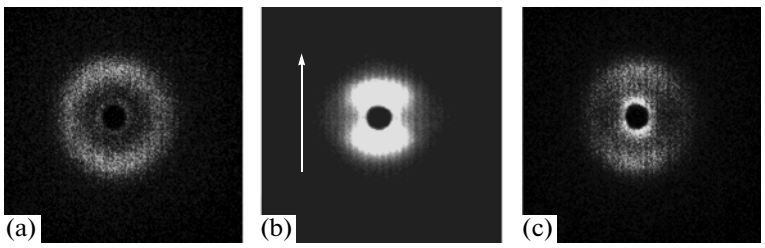

Fig. 6. SAXS patterns of (a) the initial PP-1 sample, (b) the polymer sample stretched in the medium of supercritical carbon dioxide by 100%, and (c) the latter sample after its shrinkage in the free state. The arrow shows the direction of tensile drawing of the sample.

owing to diffraction of X-ray rays on the set of fine crazes, whose long axis is primarily perpendicular to the direction of tensile drawing. An analysis of the profiles of the meridional scattering (intense smearing of an azimuthal X-ray reflection) makes it possible to conclude that the long axis of crazes in the PP sam-

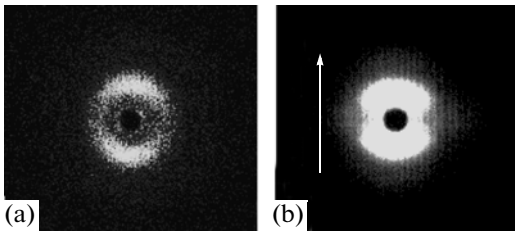

Fig. 7. SAXS patterns of (a) the initial PP-2 sample and (b) the polymer sample stretched by 100% in the medium of supercritical CO_2. The arrow shows the direction of tensile drawing of the sample.

ples, unlike the long axis of crazes in glassy polymers, is not strictly perpendicular to the direction of tensile drawing. According to our estimates, the normal to the craze surface is located at angles varying from −30° to +30° with respect to the direction of tensile drawing. The equatorial scattering is likely due to a set of craze fibrils that are oriented along the direction of tensile drawing and bridge the opposite craze walls.

The shrinkage of the PP samples is accompanied by the closure of crazes and leads to the complete recovery of SAXS patterns that are typical of the initial undeformed polymer (Fig. 6c).

The SAXS patterns of the initial PP samples and the PP samples stretched in CO_2 were used to estimate the meridional (along the direction of tensile drawing) and equatorial (in the direction perpendicular to the direction of tensile drawing) distributions of the SAXS intensity. Figures 8–10 show the corresponding curves. The SAXS intensity distribution curves in the meridional directions show a diffuse character for the stretched PP-1 samples (Fig. 8). However, the corresponding curves for the CO_2-crazed anisotropic PP samples demonstrate an interference maximum and, in some case, the intensity of this maximum is 1–1.5 orders of magnitude greater than the intensity of the meridional X-ray reflection of the undeformed polymer (Fig. 9). The key factor responsible for the intensity of the small-angle X-ray diffraction on the periodic structure is known to be the difference in the electron density of its alternating elements. Therefore, it may be expected that the development of intense X-ray reflections is due to the X-ray diffraction on the periodic structure formed by alternating regions of the bulk polymer and crazes, i.e., units that have appreciably different electron densities.

The values of the long period that correspond to angular positions of the maxima on the scattering curves were calculated according to the Wolf–Bragg equation. Figure 11 presents the long period plotted against the relative tensile strain. Note that, in this case, the long period L characterizes the distance between the centers of the microcracks; i.e., it represents the sum of the widths of the microcracks and the region of the undeformed material between the microcracks. The long period increases as the relative tensile

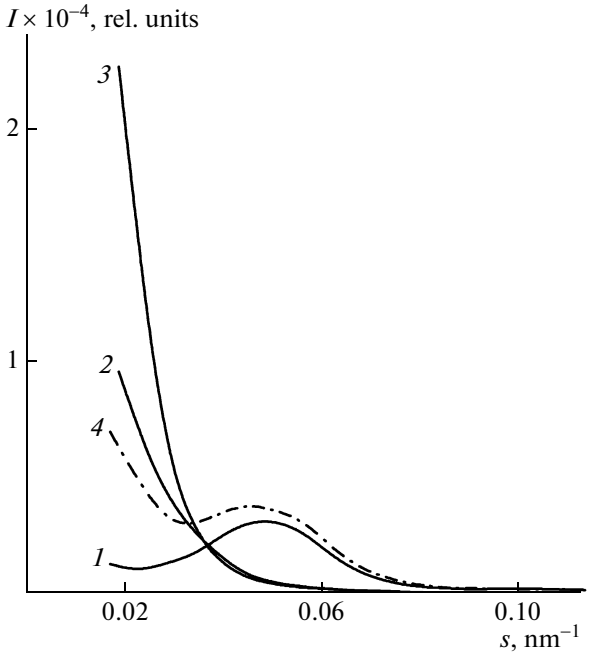

Fig. 8. The meridional SAXS intensity curves (*1*) for the initial PP-1 film, (*2–3*) for the polymer samples after tensile drawing in the medium of supercritical CO_2 by (*2*) 50 and (*3*) 100%, and (*4*) for the sample after tensile drawing in supercritical CO_2 and shrinkage in the free state. The intensities of curves *1* and *4* are increased by a factor of 200.

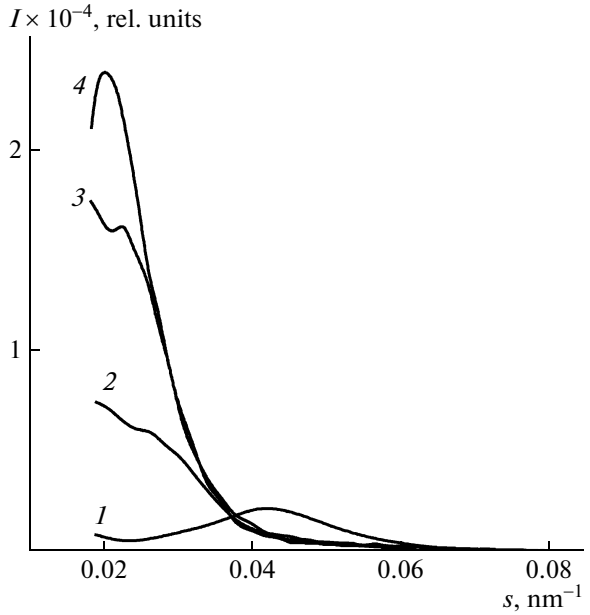

Fig. 9. The meridional SAXS intensity curves (*1*) for the initial PP-2 sample and (*2–4*) for the polymer samples after tensile drawing in the medium of supercritical CO_2 by (*2*) 50, (*3*) 60, and (*4*) 90%. The intensity of curve *1* is increased by a factor of 150.

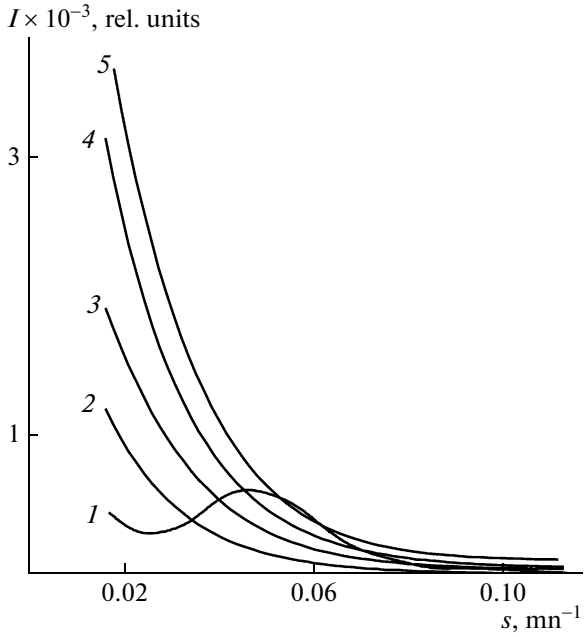

Fig. 10. The equatorial SAXS intensity curves (*1*) for the initial PP-1 film and (*2–5*) for the polymer samples after tensile drawing in the medium of supercritical CO_2 by (*2*) 50, (*3*) 60, (*4*) 100, and (*5*) 150%. The intensity of curve *1* is increased by a factor of 50.

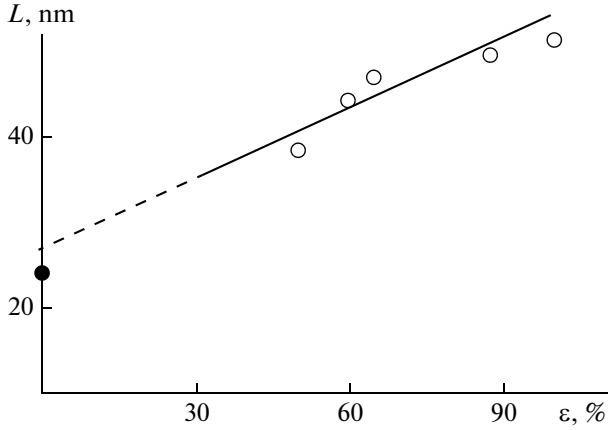

Fig. 11. The long period plotted against relative tensile strain for the PP-2 sample after its tensile drawing in the medium of supercritical CO_2. See text for explanations.

strain of the polymer increases after tensile drawing in CO_2, a result that is likely due to an increase in the craze width. The long period estimated via extrapolation of this dependence to zero tensile strain was 24 nm, a value that corresponds to the long period of the initial undeformed polymer (Fig. 11, the dark point). In turn, this result makes it possible to conclude that the nucleation and subsequent growth of crazes during the tensile drawing of PP samples in CO_2 are due to the simultaneous and regular shift (separation) of lamellas that are mainly perpendicular to the direction of tensile drawing, so that crazes by themselves are localized in the interlamellar regions of the crystalline polymer. Figure 12 shows the scheme of the structure of regions in the crystalline polymer that have a regular arrangement of crazes. The absence of diffraction maxima on the curves of meridional intensity distribution I–s of the deformed PP-1 sample (Fig. 8) is apparently due to the marked dispersion in distances between crazes parallel to direction of tensile drawing.

The SAXS intensity distribution curves recorded in the equatorial direction for the isotropic and anisotropic PP samples are diffuse (Fig. 10). This publication presents the curves only for the isotropic PP-1 samples after tensile drawing in CO_2, because the profiles of corresponding curves for anisotropic PP-2 samples are similar. As the tensile strain of polymer samples increases, the shape of the equatorial reflection remains almost unchanged, although its intensity increases. This increase apparently indicates an increase in the weight fraction of the fibrillar material during the development of crazes in the PP samples.

To calculate the key parameters of the set of crazes in the test samples (the specific surface of craze fibrils, the volume concentration of the craze fibrils, the volume of the fibrillar material, and the diameter of craze fibrils), we used the method of absolute SAXS intensity measurements [25]. In this case, we used equatorial curves recorded on the SAXS setup with the slit collimation system.

Figure 13 presents the typical equatorial scattering curves in s^2–ln$I$ coordinates recorded with the slit chamber for the PP-1 sample after tensile drawing in supercritical CO_2 by 100%. Note that the intensity function recorded with the slit chamber in the equatorial direction is the superposition of scattering from the two types of structural elements: crazes (meridional X-ray reflection) and craze fibrils in the crazes (equatorial X-ray reflection). An analysis of the SAXS patterns shows that, in the region of low scattering angles $\varphi < 20'$ ($s < 0.038$ nm^{-1}), the main contribution to the intensity of the detected scattering during scans in the equatorial direction is provided by the meridional component. However, the azimuthal length of this component quickly decreases as φ increases; at angles $\varphi > 25'$ ($s > 0.047$ nm^{-1}), it may be concluded that the equatorial intensity distribution for the PPE samples stretched in CO_2 is controlled by the internal structure of crazes, namely, by the lateral dimensions and mutual arrangement of craze fibrils.

To estimate the structural parameters of craze fibrils, scattering due to the meridional component is subtracted from the equatorial scattering curve. Later, the difference scattering was analyzed. Resolution of the components was performed in Guinier coordinates (s^2–ln$I$) under the assumption that the overall scattering includes the corresponding terms described by linear functions of the form $\ln I = A + Bs^2$ [26].

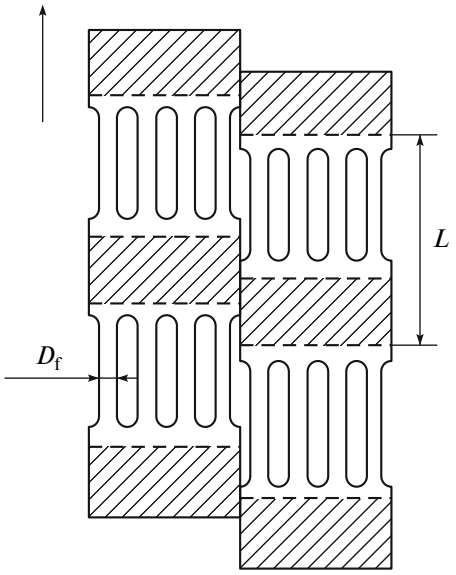

Fig. 12. The scheme illustrating the development of crazes in the PP samples during tensile drawing in the medium of supercritical CO_2. The arrow shows the direction of the tensile drawing of the sample.

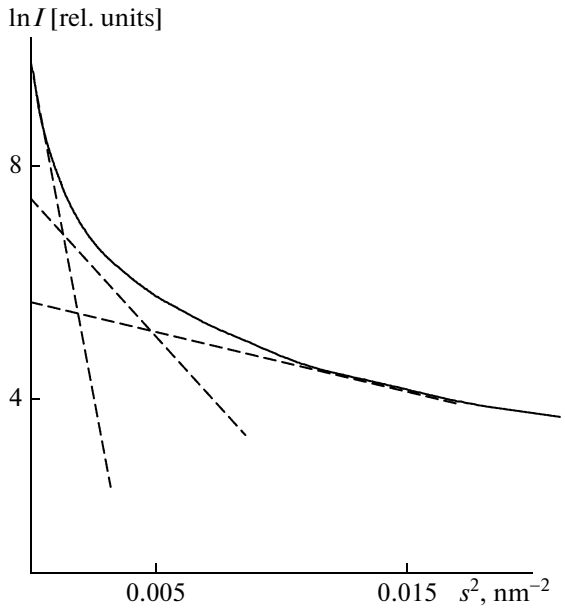

Fig. 13. The equatorial SAXS intensity distribution curves for the PP-1 sample after tensile drawing by 100% in the medium of supercritical CO_2 in s^2–ln$I$ coordinates. The curve was collected with the slit collimation system.

With consideration for the fact that the meridional component does not provide a marked contribution to the overall scattering curve at angles greater than 20′–25′ ($s > 0.047$ nm^{-1}), it is assumed that the curve with a higher slope reflects the contribution from this component to the equatorial scattering. The equatorial SAXS intensity distribution curve obtained after the subtraction of the meridional component is shown by the dashed line in Fig. 13.

It is known [26] that the invariant of the equatorial scattering curve, Q ($Q = \int_{-\infty}^{+\infty} Isds$), for the set of the parallel craze fibrils can be presented as

$$Q = c(1-c)V^*(\Delta\eta)^2$$

Here, c is the volume concentration of the fibrillar material in the crazes, $\Delta\eta$ is the difference in the electron densities of the material of the craze fibrils and the surrounding medium, and V^* is the volume fraction of the material occupied by the crazes. In this case,

$$V^* = \frac{\Delta V}{(\Delta V + V_0)(1-c)},$$

where ΔV is a change in the volume of the crazed sample relative to the volume of the initial undeformed sample. The Q value is independent of the diameter of the craze fibrils.

With the use of Porod invariant Q measured in absolute units and void-volume gain $\Delta V/V_0$ formed during tensile drawing of the PP samples in contact with supercritical CO_2, the above relationships were used to calculate the volume concentration of the fibrillar material in the crazes. The values of parameter c were used for calculation of craze-fibril volume V_f normalized by the volume of the undeformed sample

$$V_f = c\frac{\Delta V/V_0}{1-\Delta V/V_0}$$

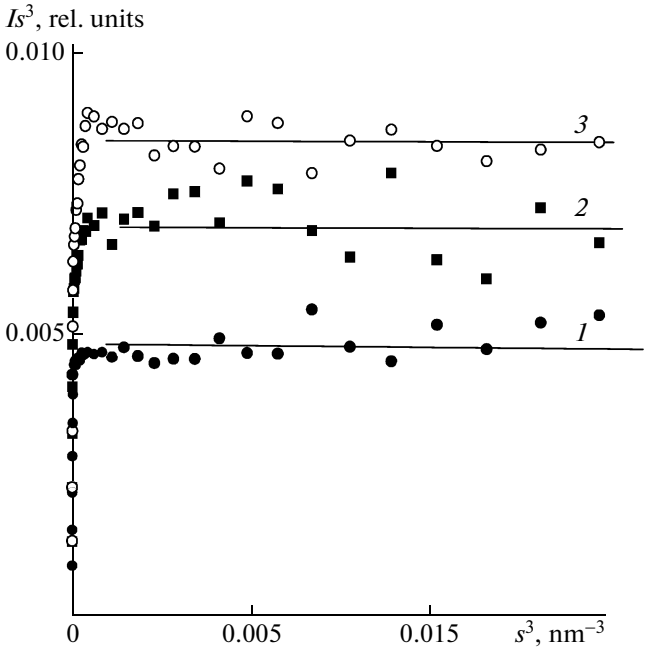

Fig. 14. Porod curves in Is^3–s^3 coordinates for the PP-1 samples after tensile drawing in the medium of supercritical CO_2 by (*1*) 50, (*2*) 100, and (*3*) 150%.

Characteristics of the microporous structure of PP-1 and PP-2 films after uniaxial tensile drawing in the medium of supercritical CO_2 at a pressure of 10 MPa and a temperature of 35°C

Tensile strain, %	Volume gain $\Delta V/V_0$, rel. units	Volume concentration of the craze fibrils, c, rel. units	Specific volume of fibrils V_f, rel. units	Specific surface of fibrils S_f, m^2/cm^3	Diameter of fibrils D_f, nm
			PP-1		
50	0.25	0.38	0.15	60	10.0
100	0.40	0.39	0.26	100	10.0
150	0.45	0.41	0.31	120	10.0
			PP-2		
50	0.26	0.26	0.09	40	9.0
75	0.35	0.29	0.15	70	8.5
100	0.40	0.35	0.22	90	10.0

The surface of the craze fibrils, S_f, bridging the opposite craze walls was estimated according to the Porod method (modified for oriented systems) through analysis of the tail part of the equatorial X-ray scattering curve [25, 26]. The equatorial scattering curves plotted in Is^3–s^3 coordinates for the PP samples after tensile drawing in supercritical CO_2 are presented in Fig. 14. In the interval of large scattering angles, product Is^3 is constant. This profile of the curve agrees with the theoretical calculations of the scattering function from the set of oriented fibrils, $I \sim k/s^3$, where k is a parameter proportional to the surface area of the craze fibrils (the Porod constant) [26]. The fact that Is^3 is constant in the interval of large values of s is indicative of the sufficient sharpness of the phase boundaries between the craze fibrils. As follows from Fig. 14, the Porod constant increases as the tensile strain of the PP samples increases during tensile drawing in supercritical CO_2.

The surface area of the craze fibrils normalized by the volume of the initial sample was calculated with the equation advanced in [25, 26]:

$$S_f = \frac{2\pi^2 k\lambda^2}{(\Delta\eta)^2}(1 + \Delta V/V_0) \text{ at } k = \lim_{s\to\infty} Is^3$$

The diameter of the craze fibrils was calculated from the values of the specific volume and the specific surface of the craze fibrils:

$$D_f = 4V_f/S_f$$

The results of calculating the structural parameters of the crazes formed during the tensile drawing of the PP samples in supercritical CO_2 are summarized in the table. The parameters of the crazes are practically the same for both types of the PP samples. In this case, the crazes formed during the tensile drawing of PP films in supercritical CO_2 posses a highly disperse structure and a highly developed surface. The diameter of the fibrils bridging the opposite craze walls is ~10 nm, and the specific surface of the craze fibrils in the samples stretched by 100–150% is 100–120 mm^2/cm^3.

Therefore, the tensile drawing of semicrystalline PP in the medium of supercritical CO_2 proceeds via the mechanism of delocalized solvent crazing and leads to the development of an open porous fibrillar structure on the nanoscale level of dispersion. The parameters of the porous structure approach the corresponding parameters of the solvent-crazed PP samples prepared by crazing in traditional AALEs. We believe that the preparation of porous polymers and nanocomposites in the presence of supercritical media is a promising direction in materials science because the characteristics of a medium can be smoothly changed through variation in the temperature and pressure and the process itself is environmentally friendly.

ACKNOWLEDGMENTS

We would like to thank A.N. Ozerin, S.N. Chvalun, and T.S. Kurkina for their help with X-ray structural measurements.

REFERENCES

1. I. Narisava, *Strength of Polymer Materials* (OHMSHA, 1982; Khimiya, Moscow, 1987).
2. A. L. Volynskii and N. F. Bakeev, *Solvent Crazing of Polymers* (Elsevier, Amsterdam, 1995).
3. R. P. Kambour, J. Polym. Sci., Part D: Macromol. Rev. **7**, 1 (1973).
4. L. M. Yarysheva, A. L. Volynskii, and N. F. Bakeev, Polymer Science, Ser. B **35**, 1000 (1993) [Vysokomol. Soedin., Ser. B **35**, 913 (1993)].
5. A. L. Volynskii, O. V. Arzhakova, L. M. Yarysheva, and N. F. Bakeev, Polymer Science, Ser. B **42**, 70 (2000) [Vysokomol. Soedin., Ser. B **42**, 549 (2000)].
6. A. L. Volynskii, A. Sh. Shtanchaev, and N. F. Bakeev, Vysokomol. Soedin., Ser. A **26**, 2445 (1984).
7. E. A. Shmatok, L. M. Yarysheva, A. L. Volynskii, and N. F. Bakeev, Vysokomol. Soedin., Ser. A **31**, 1752 (1989).

8. H. G. Olf and A. Peterlin, J. Polym. Sci., Part B: Polym. Phys. **12**, 2209 (1974).
9. N. Brown and B. D. Metzger, J. Polym. Sci., Part B: Polym. Phys. **18**, 1979 (1980).
10. A. L. Volynskii, L. M. Yarysheva, E. M. Ukolova, et al., Vysokomol. Soedin., Ser. A **24**, 2614 (1987).
11. M. A. McHugh and V. J. Krukonis, *Supercritical Fluid Extraction: Principles and Practice* (Butterworth-Heineman, Stoneham, 1993).
12. T. Hobbs and A. J. Lesser, J. Polym. Sci., Part B: Polym. Phys. **37**, 1881 (1999).
13. M. Garcia-Leiner, J. Song, and A. J. Lesser, J. Polym. Sci., Part B: Polym. Phys. **41**, 1375 (2003).
14. X. Hu and A. J. Lesser, J. Cell. Plast. **42**, 517 (2006).
15. K. Hirogaki, I. Tabata, K. Hisada, and T. Hori, J. Supercrit. Fluids **38**, 399 (2006).
16. E. S. Trofimchuk, A. V. Efimov, L. N. Nikitin, et al., Dokl. Akad. Nauk **428**, 480 (2009).
17. A. L. Volynskii, N. F. Bakeev, L. M. Yarysheva, et al., RF Patent No. 2382057 (2008).
18. A. V. Efimov, V. P. Lapshin, P. V. Kozlov, and N. F. Bakeev, Vysokomol. Soedin., Ser. A **23**, 882 (1981).
19. A. V. Efimov, N. N. Valiotti, V. N. Dakin, et al., Vysokomol. Soedin., Ser. A **30**, 963 (1988).
20. E. A. Sinevich, I. V. Bykova, and N. F. Bakeev, Polymer Science, Ser. B **40**, 327 (1998) [Vysokomol. Soedin., Ser. B **40**, 1671 (1998)].
21. Zh.-M. Xu, X.-L. Jiang, T. Liu, et al., J. Supercrit. Fluids **41**, 299 (2007).
22. X.-L. Jiang, T. Liu, Zh.-M. Xu, et al., J. Supercrit. Fluids **48**, 167 (2009).
23. A. V. Efimov, V. P. Bondarev, P. V. Kozlov, and N. F. Bakeev, Vysokomol. Soedin., Ser. A **24**, 1690 (1982).
24. S. L. Cannon, G. B. McKenna, and W. O. Statton, J. Polym. Sci., Part D: Macromol. Rev. **11**, 209 (1976).
25. A. V. Efimov, V. M. Bulaev, A. N. Ozerin, et al., Vysokomol. Soedin., Ser. A **28**, 1750 (1986).
26. E. Paredes and E. W. Fischer, Makromol. Chem. **180**, 2707 (1979).